Title: Laser-treated electrospun fibers loaded with nano-hydroxyapatite for bone tissue engineering

Authors: Javier Aragon, Nuria Navascues, Gracia Mendoza, Silvia Irusta

PII: S0378-5173(17)30312-5
DOI: http://dx.doi.org/doi:10.1016/j.ijpharm.2017.04.022
Reference: IJP 16588

To appear in: *International Journal of Pharmaceutics*

Received date: 11-11-2016
Revised date: 7-4-2017
Accepted date: 10-4-2017

Please cite this article as: Aragon, Javier, Navascues, Nuria, Mendoza, Gracia, Irusta, Silvia, Laser-treated electrospun fibers loaded with nano-hydroxyapatite for bone tissue engineering.International Journal of Pharmaceutics http://dx.doi.org/10.1016/j.ijpharm.2017.04.022

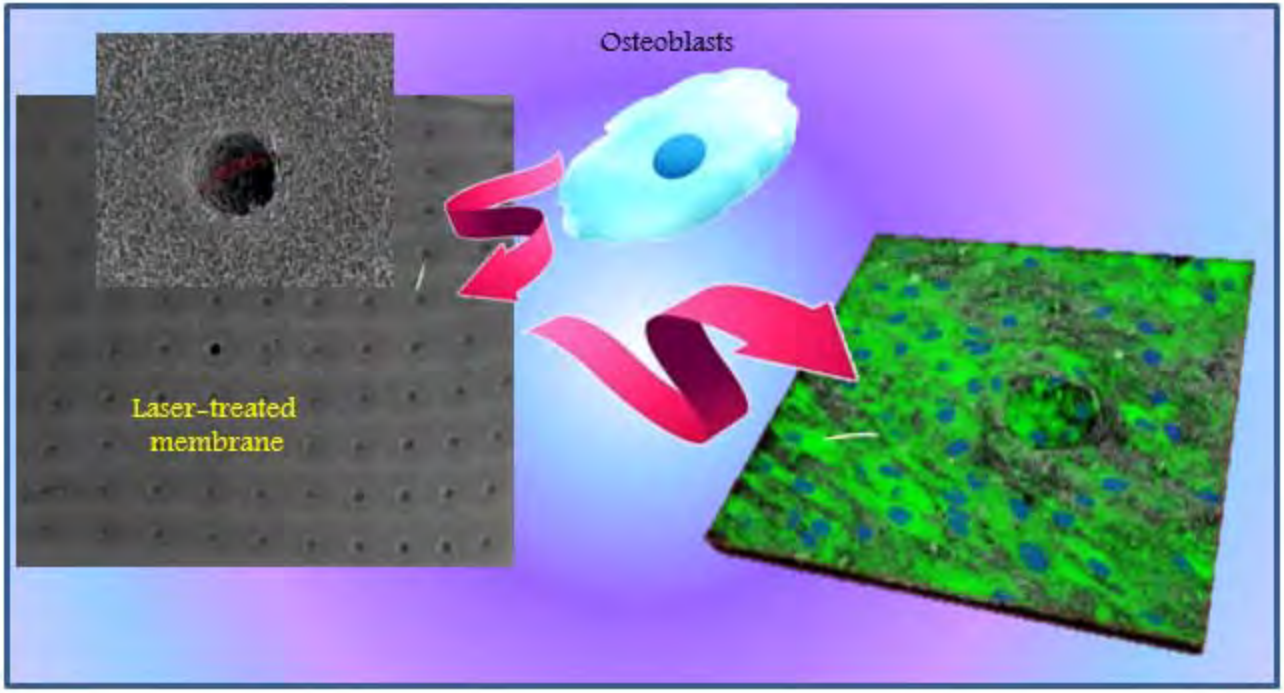
Osteoblasts
Laser-treated
membrane

Laser-treated electrospun fibers loaded with nano-hydroxyapatite for bone tissue engineering

Javier Aragon[1], *Nuria Navascues*[1], *Gracia Mendoza*[1,*], *Silvia Irusta*[1,2,*]

[1] Department of Chemical Engineering, Nanoscience Institute of Aragon (INA), University of Zaragoza,50018 Zaragoza, Spain.

[2] Networking Research Center on Bioengineering, Biomaterials and Nanomedicine, CIBER-BBN, 28029 Madrid, Spain.

KEYWORDS: Bone regeneration, scaffold, laser treatment, electrospinning, nanohydroxyapatite.

ABSTRACT

Core-shell polycaprolactone/polycaprolactone (PCL/PCL) and polycaprolactone/polyvinyl acetate (PCL/PVAc) electrospun fibers loaded with synthesized nanohydroxyapatite (HAn) were lased treated to create microporosity. The prepared materials were characterized by XRD, FTIR, TEM and SEM. Uniform and randomly oriented beadless fibrous structures were obtained in all cases. Fibers diameters were in the 150-300 nm range. Needle-like HAn nanoparticles with mean diameters of 20 nm and length of approximately 150 nm were mostly encase inside the fibers. Laser treated materials present micropores with diameters in the range 70-120 μm for PCL-HAn/PCL fibers and in the 50-90 μm range for PCL-HAn/PVAC material. Only samples

containing HAn presented bioactivity after incubation during 30 days in simulated body fluid. All scaffolds presented high viability, very low mortality, and human osteoblast proliferation. Biocompatibility was increased by laser treatment due to the surface and porosity modification.

1. INTRODUCTION

Scaffolds are specially designed biomaterials that provide a support for cell growth, migration and finally proliferation to allow tissue regeneration (Joshi et al., 2016). In order to satisfy the required adhesion and proliferation of cells geometric factors are of great importance (Pereira et al., 2014). The matrix architecture is vital for the success of bone tissue engineering which includes microstructure of scaffold, its porosity percentage and surface topography (Uma Maheshwari et al., 2014). Polymer nanofibers obtained by electrospinning mimic the bone extracellular matrix structure and the potential to enhance the osseointegration is very promising (Song et al., 2013). They also exhibit high surface area to volume ratios favourable for cells and bioactive molecules attachment to the fibers surface. However, the small pore size of electrospun scaffolds hinders cell infiltration and ultimately reduces their use in replacing large tissues that require ample vascularization and nutrient diffusion (Lee et al., 2012). To promote cellular viability and extracellular matrix production, electrospun scaffolds with enhanced porosity or micro-scale pores could be beneficial since increasing porosity and pore size can provide a three-dimensional (3D) environment that not only facilitates cell seeding/diffusion but also provides better diffusion of nutrients and waste throughout the scaffolds (Suwantong et al., 2014).

Different techniques were studied to obtain electrospun materials with larger pores or higher porosity. Among them the addition of porogens during electrospinning and the posterior elimination by leaching was used (Kim et al., 2008). Collection in liquid increases the pore size but the fabrication is highly dependent on the surface tension, flow rate and weight fraction of the polymer solution (Kim and Kim, 2014a). Another promising technique to improve electrospun materials porosity is the surface modification by laser technologies for scaffold microstructuring. Laser has become an invaluable tool in processing and treating biological

tissues due to its possibility of precise material processing with clean surfaces and reduced thermal damage. Pulsed laser ablation is a well-established universal tool for direct surface modification of almost all type of materials. Ultra-short laser pulses (picosecond and femtosecond) enable to obtain 3D microstructures with high precision, taking advantage of the "cold" ablation process (Ortiz et al., 2014). It was demonstrated that laser machining is an efficient technique to prepare patterning structures in electrospun polycaprolactone (PCL) membranes (Choi et al., 2007; Wu et al., 2011). It was found that electrospun poly(l-lactide) scaffolds with laser ablated holes exhibit significant better endothelial cell ingrowth (Lee et al., 2012). McCullen et al. (McCullen et al., 2011) used laser ablation on electrospun PCL scaffolds to favour the adhesion and growth of human adipose-derived stem cells. Electrospun PCL/β-TCP fibers were also treated by laser irradiation to obtain microsized pores (Kim and Kim, 2014b). Beside the meaningful cellular activity the material showed enhanced compressive strength.

Naturally occurring polymers are well suited for various *in vivo* applications, promoting cell adhesion and growth. However, scaffolds fabricated from these polymers could exhibit poor mechanical properties or fast degradation rates. Native proteins, such as collagen and fibrinogen, are also more expensive and more difficult to source than synthetic polymers (Baker et al., 2016). Among the synthetic available polymer used to fabricate three-dimensional (3D) scaffolds aliphatic polyesters undoubtedly represent so far the most extensive studied class, since they combine good physico-chemical and mechanical properties with assessed biocompatibility (Chen et al., 2016). Particularly PCL is a low cost, biocompatible polymer that has a slow degradation rate and distinct rheological and viscoelastic properties that make it suitable for specific long term implantation (Baker et al., 2016). Its compatibility with a wide range of drugs enables uniform drug distribution in the matrix and its long term degradation facilitates drug release up

to several months (Dash and Konkimalla, 2012). Polyvinyl acetate (PVAc) polymer has also been applied in many medical fields because of its strong biocompatibility. The hydrogels containing functional groups such as COOH usually show good biocompatibility with blood, body fluids, and tissues (Ha et al., 2013). This inert polymer has the advantage that it does not induce a deleterious reaction in living tissue (Sadato et al., 1994). Because of all these characteristics PVAc has been used in many medical fields, including drug and cell carries and in tissue engineering (Abdal-hay et al., 2015).

One important limitation in the use of synthetic biodegradable polymers as scaffold materials is the lack of bioactivity, in particular for bone tissue applications (Aragon et al., 2011). The main approach to develop bioresorbable and bioactive scaffolds is the addition of bioactive materials to the polymer matrix. Calcium phosphate ceramics have been extensively investigated to fabricate highly porous scaffolds to engineer bone due to their near similar composition of bone, including excellent biocompatibility, osteoinductive and osteoconductive properties (Uma Maheshwari et al., 2014). It has been found that the addition of hydroxyapatite (HA) not only enhances the tensile strength of PCL scaffolds but also acts as a chelating agent to accelerate the mineralization of human fetal osteoblast cells to form bone-like apatite for bone tissue engineering (Jing et al., 2015).

In this work core shell PCL/PVAc and PCL membranes were obtained by electrospinning. The fibers were loaded with synthetic hydroxyapatite nanoparticles (HAn) to increase the bioactivity of the materials. The prepared scaffolds were then treated by laser ablation to create desired microscale topographical features in order to favour cell adhesion and growth. The materials were characterized by scanning electron (SEM) and transmission electron (TEM) microscopies and X-ray powder diffraction (XRPD). The bioactivity was also tested. The effect of porosity

from patterned holes on cell adhesion morphology and proliferation *in vitro* was studied. There are few publications dealing with the use of laser ablation to improve scaffolds porosity, and to the authors knowledge none that apply this technique in PCL/PVAc fibers loaded with HAn.

2. EXPERIMENTAL SECTION

2.1. Materials

PCL and PVAc with an average molecular weight of 80000 Da and 140000 Da respectively, dicloromethane (DCM), N,N-dimethylformamide (DMF), calcium carbonate ($CaCO_3$), phosphoric acid (H_3PO_4), ammonium hydroxide solution (NH4OH), TWEEN® 80 and CellCrown™ inserts (24 well plate inserts) were purchased from Sigma-Aldrich (Spain). Clonetics™ OGM™ osteoblast growth medium (OGM), trypsin-EDTA and Clonetics™ normal human osteoblasts (NHOst) were purchased from Lonza (Belgium). Dulbecco's phosphate-buffered saline (DPBS) were purchased from Biowest (France).

2.2. Synthesis of hydroxyapatite nanoparticles

Synthesis of HA ($Ca_{10}(PO_4)_6(OH)_2$) nanoparticles was conducted as previously described (Paz et al., 2012). $CaCO_3$ was used as calcium sources, maintaining a Ca/P ratio of 1.67 during reaction in solution with 0.3 M H_3PO_4.

2.3. Preparation of electrospun scaffolds

Electrospun scaffolds were prepared using an Yflow 2.2.D-500 electrospinner (Coaxial Electrospinning Machines/R&D Microencapsulation, Malaga, Spain). PCL pellets were dissolved in DCM/DMF (1:1) and PVAc was dissolved in DMF, these solutions were stirred

overnight at room temperature. To prepare PCL-HAn scaffolds, HAn powder was dispersed in DCM/DMF with the help of TWEEN® 80 by stirring overnight at room temperature, then this solution was added to the PCL solution and stirred overnight at room temperature. The polymers solutions were loaded into 20 mL plastic syringes. The PCL-HAn suspension was fed through the inner needle of the coaxial system and PCL or PVAc solutions were fed through the outer one. This last needle was connected to the positive voltage power supply, at a voltage ranging from 7 to 13 kV. The shell and core flow rates and the spinning distance were fixed to 0.5 mL/h (in both needles) and 19 cm respectively. The spun fibers were collected on a static plate (covered with aluminum foil) connected to negative voltage power supply, at a voltage ranging from -2 to 4 kV for 18 hours. To create macropores in the fibrous membrane structures, a pulse Nd:YAG laser (TECHNOLOGY Q-Switch) was used. Different conditions were used for each material: output power: 16 W, wavelength: 1064 nm for the PCL-HAn/PCL fibers and output power: 1 W, wavelength: 532 nm for PCL-HAn/PVAc fibers.

2.4. Physicochemical characterization

Morphology of HAn and electrospun fibers was analyzed using a TEM microscope operated at 300 kV (Tecnai F30, FEI, USA) and SEM microscope (Field Emission Scanning Electron Microscope CSEM-FEG INSPECT 50, FEI, USA). The size distribution statistics were obtained by measuring at least 100 fibers or particles in different images. Fourier transform infrared (FTIR) spectrum and XRPD were used to evaluate the molecular structure and to identify the crystallographic phases of the HAn. FTIR spectra were recorded using a Vertex-70 FTIR spectrophotometer (Brucker, USA). The powder diffraction pattern was measured in a diffractometer (Rigaku RINT 2000) with a monochromatic Cu Kα radiation.

Scaffolds thermal analyses were conducted with a thermogravimetric analyzer (TGA) from METTLER TOLEDO (TGA/SDTA 851e). A mercury porosimeter (POREMASTER, Quantachrome), was used in the experiments of mercury intrusion. At least five samples were tested for each type of membrane.

2.5. *In vitro* studies in simulated body fluid (SBF)

In vitro studies in simulated body fluid (SBF) were carried out using the SBF composition and the standard procedures described by Kokubo and Takadama (Kokubo and Takadama, 2006). Electrospun scaffolds membranes were immersed in 10 mL of SBF for 30 days at 37 °C and, every 72 hours in the first 15 days and every week in the last 15 days, the liquid phase was replaced with 10 mL of fresh SBF. After immersion in SBF the samples were characterized by SEM to verify whether HA was formed on the surfaces of the scaffolds.

2.6. Cell culture

Electrospun scaffolds membranes were fixed in CellCrown™, sterilized by UV-irradiation for 30 minutes on both sides and rinsed overnight with OGM. Normal human osteoblasts (NHOst, Lonza, Belgium) were grown in OGM culture medium, supplemented with 10 % FBS, ascorbic acid and 5 % solution of gentamicin and amphotericin-B (OGM BulletKit, Lonza, USA) as the manufacturer indicates in an atmosphere containing 5 % CO_2 at 37ºC. Electrospun scaffolds membranes fixed in CellCrown™ were incubated for 12-18 h in OGM. Then, culture medium was removed and NHOst at passages between 5 and 6 were seeded on the scaffolds at a density of $3{,}2x10^6$ cells/mL suspended in 10 μL of medium on the scaffolds center. Samples were incubated for 1 h and then more OGM was added to each well. Next, the cells were cultured up to 2, 7 and 14 days, renewing the culture medium every 2 days.

2.7. Cell viability

A Live/Dead® Viability/Cytotoxicity Kit *for mammalian cells* (Molecular Probes, UK) was used to determine cell viability after 48h, 7 and 14 days of cultivation, according to the manufacturer's protocol. Calcein-AM was used as a marker of esterase activity in living cells, EthD-1 penetrates into dead cells through their damaged membrane and produces red fluorescence and cellular nuclei were stained with an anthraquinone dye (DRAQ5TM). The scaffolds were washed with DPBS five times for five minutes every time and incubated in 0.5 mL of Live/Dead® working solution and 8 μM of DRAQ5. Staining was performed under dark conditions for 30 min at room temperature. Imaging the sample surfaces and cellular morphology were obtained on a confocal laser scanning microscope (Leica TCS SP2).

2.8. Image processing for cell viability quantification

Image J software (Version 1.48f , NIH, US) was used to quantify the viability of NHOst seeded onto the different scaffolds described above. Confocal images were analyzed through a step-by-step procedure on the green channel as it recorded the live cells, setting up the scale and the threshold in this channel. Cell viability was determined by the ratio of green pixel area to the total area of pixels. Five different regions of each sample were evaluated and the maximum projection of at least 60 planes per region was quantified (total area analyzed per region ≈ 0.14 cm^2). Semiautomatic measurement was developed to calculate the percentage of the covered area by live cells stained with calcein.

2.9. Cell morphology

SEM was performed to observe cell morphology and attachment on electrospun scaffolds membranes. After 48 h, 7 and 14 days of cultivation samples were washed with DPBS, fixed in a 4% paraformaldehyde solution at room temperature for 30 minutes. The samples were sputter-coated with platinum and characterized by SEM microscopy (Field Emission Scanning Electron Microscope CSEM-FEG INSPECT 50, FEI, USA).

2.10. Statistical analysis

All mechanical and release data were expressed as mean±standard deviation (SD) for n=5 (for fiber diameter n=100 and for image analysis 60 planes per region and 5 regions per sample) and were analyzed using standard Student's t-test analysis. Differences were considered significant when $p \leq 0.05$.

3. RESULTS AND DISCUSSION

3.1. Hydroxyapatite characterization

The XRD pattern for the synthesized HA nanoparticles is shown in Figure 1 a, it could be seen that all the peaks could be indexed to the hexagonal phase hydroxyapatite (JCPDS Nº 09-0432). The diffractogram do not show any other peaks corresponding to secondary phases or intermediate compounds suggesting the formation of pure HAn phase. Intense diffraction peaks with broad width are indicative of the crystalline nature of the prepared material and the small crystallite size respectively (Mohandes et al., 2014). Inset of Figure 1a shows the peaks corresponding to the (002) and (211) diffraction planes of hydroxyapatite. According to the JCPDS card 09-0432, the reference intensity ratio for (211), (002) is RI(211)/ RI(002)= 2.61. The calculated degree of texture index (David Nunez et al., 2014) for the synthesized

hydroxyapatite is 0.51 indicating a preferred growth orientation along the c-axis (Nathanael et al., 2015). These results are consistent with electronic microscope images (Figure 1 b and c), which show fibrous needle-like particles with mean diameters of 20 nm and length of approximately 150 nm. The rod-like shape of the nanoparticles is more clearly seen in TEM images (Figure 1 c). The FTIR spectrum of the material presents the characteristic bands for PO43- appearing at 472, 572 and 603cm^{-1} related to the asymmetric bending, and signals assigned to symmetric and asymmetric stretching positioned in the 900-1200 cm^{-1} range (Taheri et al., 2015). The broad peak around 3455 cm^{-1} is due to the adsorbed water on HAn structure and the absorption peak at 1635 cm^{-1} is attributed to the bending mode of OH^- groups (Mary et al., 2016). The absorption peak assigned to apatite hydroxyl bond is observed at 3569 cm^{-1} (An et al., 2016). The shoulder at 878 cm^{-1} together with the doublet at 1415 and 1458 cm^{-1} indicate the existence of CO_3^{2-} (Dai et al., 2015) probably coming from the atmosphere carbon dioxide during sample preparation and would have been incorporated into the HAn crystal structure (Verma et al., 2013). All these results imply that the synthesis of rod-like shaped hydroxyapatite nanoparticles was successful.

Scaffolds characterization

3.1.1. As spun scaffolds

The materials prepared by electrospinning are listed in Table 1 together with positive and negative voltages applied. Due to the properties (viscosity, surface tension, conductivity) of the solutions the voltages required to obtain a stable Taylor cone were higher to produce fibers containing hydroxyapatite than the voltages used for the pristine polymer fibers (Table 1).

The HAn load in the fibers was measured by thermogravimetric analysis (TGA, Figure SI 1) as the residue after complete polymers elimination at 600 ºC (Table 1). The experimental values of 13.8 and 12.7 wt% for PCL-HAn/PCL and PCL-HAn/PVAC respectively, were close to the theoretical ones (13.2 and 11.9 wt%). The HAn load used was the maximum possible to obtain a stable Taylor cone; higher amount of nanoparticles in the spinning solution increase excessively the viscosity and also hinder good nanoparticles dispersion.

Table 1: Preparations conditions and characterization results for the obtained electrospun scaffolds.

Sample (Core/Shell)	Applied voltage -/+ (kV)	HAn load (wt%)[1]	Fiber diameter[2] (nm)	Porosity	Pores diameter (nm)
PCL/PCL	3.11/10.25	-	206±62	62.0%	232
PCL-HAn/PCL	3.54/12.00	13.8 (14.2)	210±64	63.5%	210
PCL/PVAc	2.87/7.21	-	264±56	65.5%	209
PCL-HAn/PVAc	3.03/8.57	12.7 (11.9)	225±47	58.6%	188

[1] From TGA results, theoretical value between brackets.

[2] Obtained by measuring at least 100 fibers in different SEM images

XRD patterns of fibers with HAn are shown in Figure 2. The XRD diffractgram of PCL-Han/PCL has peaks for both hydroxyapatite and PCL. Both the polymer and ceramic retain their

crystalline behaviour in the electrospun fibers indicating insignificant change in their crystal structure. This confirms the fact that HAn is finely and uniformly dispersed in the matrix (Uma Maheshwari et al., 2014). In PCL-HAn/PVAc pattern peaks at 25 and 35º establish the presence of hydroxyapatite incorporated in the scaffold (inset of Figure 2).

FE-SEM images of the electrospun scaffolds showed uniform, beadless and nano-scaled fibrous structures randomly oriented for all the prepared materials under the optimum spinning conditions utilized in each case. As an example Figure 3 a) shows SEM micrographs obtained for fibers with PCL in the core and in the shell. Hydroxyapatite nanoparticles are mostly encased inside the fibers, but some agglomerates are observed on the surface (Figure 3 b). The fibers average diameter was measured from SEM images (Table 1). The presence of hydroxyapatite nanoparticles in the inner solution does not seem to have any effect on the PCL/PCL fiber diameter. It was previously observed for PCL fiber without defects, such as the obtained in this work, that for HA load higher than 5 wt% the average diameter was similar to the pristine fibers (Metwally et al., 2015). This result for high mass fraction was attributed to the increased viscosity of the dispersion during electrospinning. For the PCL/PVAc material the presence of hydroxyapatite leads to a slightly lower fibers mean diameter, probably due to the higher voltage needed to obtain a stable cone in the case of the hydroxyapatite loaded fibers (Cramariuc et al., 2013).

The core-shell structure of the PCL/PVAc fibers was investigated by TEM microscopy as shown in Figure 4 a. The PVAc polymer (the transparent part of the outside structure of the fiber) is the shell wrapping uniformly the PCL fiber (the darker part of the inside structure of the fiber) as the core. A TEM micrograph of a PCL/PCL fiber was added in the inset for comparison purpose, as expected core and shell are indistinguishable in this case. The distribution of the HA

nanoparticles inside fibers can be observed in Figure 4 b, as mentioned before most of the particles are encapsulated into the polymers.

3.1.2. Laser treated scaffolds

After laser irradiation the scaffolds were analysed by SEM microscopy (Figure 5). For both materials the laser energy was not sufficient to machine a hole through the electrospun fibers. The images show that the membrane was not significantly affected outside the laser irradiation area. Figure 5a shows SEM images of PCL-HAn/PCL ablated scaffolds, the micropores were well obtained with diameters in the range 70-120 μm. It is important to observe the morphology of the remaining fibers since the aim is to improve the porosity without any additional effect (Rebollar et al., 2011). Even when some melting and coalescence of the fibers can be observed around the drilled holes, the surface morphology is only slightly changed. For PCL-HAn/PVAC on the other hand, the pores diameter are in the 50-90 μm range and the change in the fibers morphology around the holes is more important. Besides, in this material not all the holes of the rectangular pattern were produced under irradiation. As mentioned in the experimental section different laser were used in order to get the pores in each material.

3.2. *In vitro* bioactivity

Biomineralization method was used in order to evaluate bone binding ability of the prepared materials. The apatite formation was monitored using the fibers pad before the laser treatment since the most important factor for the bioactivity of materials is the surface nature of fibers

(Singh et al., 2015). Figure 6 shows SEM images of both kind of fibers unloaded and hydroxyapatite loaded having been soaked in SBF for various times. Hydroxyapatite precipitation can be observed after incubation during 14 and 30 days only in samples containing HAn. The apatite form aggregates that reach size of more than 3 μm. The nanoparticles on the surface of fibers would act as nucleation sites in SBF, thus the presence of HAn is necessary for the apatite formation on the nanofiber surface. Fibers with PVAc shell suffer some structural change due to the poor water resistance of the polymer (Zhang et al., 2013), but they still exhibited a well interconnected pore network structure, which is necessary for mineral deposition and cellular in-growth. Characteristic peaks of calcium, phosphorous and oxygen, the main components of hydroxyapatite in EDX analysis (not shown) confirm the nature of the deposited aggregates. From these analyses Ca/P atomic ratios were 1.6 for PCL-HAn/PCL and 1.7 for PCL-HAn/PVAc.

3.3.*In vitro* cell morphology and viability

Human osteoblasts seeded onto the different types of scaffolds fabricated were evaluated regarding their morphology and proliferation until 14 days in order to assess their potential as bone regeneration scaffolds. SEM micrographs (Figure 7) showed cell adhesion to all the scaffolds and a normal morphology of cells which are homogenously distributed on the surface and with a clear higher cell density after 14 days especially in the scaffolds containing PVAc pointing to a good biocompatibility of the prepared materials.

To further investigate the suitability of these scaffolds for bone tissue engineering, the viability of the osteoblasts seeded was tested after 48h (Figure SI 2), 7 days (Figure SI 3) and 14 days

(Figures SI 4 and 5). It should be noted that all confocal acquisitions were performed with the same settings. Biocompatibility of our scaffolds is clearly shown exerting high viability, very low mortality, which is even diminished with time, and cell proliferation. Furthermore, the laser treatment of the surfaces notably increased the scaffolds biocompatibility observing higher viability and cell density which could be attributed to the modification of the scaffolds surface and porosity (Figure 8) even in the nanometer scale as has been described for titanium engineered surfaces due to the change in protein adsorption and thus cell adhesion and proliferation (Chu et al., 2016; Rosales-Leal et al., 2010). In all the scaffolds assayed, cell growth was recorded mostly on the seeding surface probably due to the low pore size (VIDEO SI). In this sense, nano-porosity data of the un-treated scaffolds were very similar in all the different formulations assayed as described in Table 1, pointing to this factor as the responsible of the homogeneity in the results obtained in the cell viability and proliferation studies.

Previous studies have reported the biocompatibility of PCL electrospun 3D-scaffolds in a human osteoblast *in vitro* model in which the high porosity enabled cells to penetrate into the scaffold (Wang et al., 2010). The grafting of collagen and chondroitin sulphate on modified surface PCL porous scaffolds synthesized by particulate leaching significantly increased the *in vitro* proliferation of murine chondrocytes four weeks after seeding though porosity was not altered (Chang et al., 2010) while chemically cross-linked PCL and HAn nanoparticles used to fabricate nanocomposite scaffolds loaded with the growth factor BMP-2 also showed very good cytocompatibility in a rabbit bone marrow stem cells *in vitro* model (Liu et al., 2014), supporting PCL suitability as biomedical material. In addition, the fabrication of PCL scaffolds treated with a femtosecond laser to create pores, and therefore to modify the scaffold surface and porosity, has shown enhanced cellular activities compared to those scaffolds with the same pore size and

not treated with laser (Kim et al., 2014), indicating that laser treatment may significantly improve the potential of these types of scaffolds in bone regeneration as our study shows. Though it is controversy regarding the "ideal" size pore for biomedical applications, in osteoregeneration most authors have pointed to 100-400 μm as recommended to facilitate cell adhesion and growth (Roosa et al., 2010). However, smaller pores are able to increase scaffolds surface and lead to higher cell attachment while larger pores facilitate cell migration (Kim et al., 2014). Our results showed that laser pulse on PCL-HAn/PVAc scaffolds implied the formation of micropores of 50-90 μm while on PCL-HAn/PCL were slightly larger (70-120 μm). These data, together with the apparently higher cell density recorded in PVAc containing scaffolds, suggest that smaller micropore sizes made easier cell adhesion and proliferation.

The incorporation of HAn in the synthesis process of poly(L/DL)-lactide (Rajzer et al., 2014) or polylactic acid (PLA) (Morelli et al., 2015) electrospun scaffolds for biomedical applications has been reported in order to improve cell attachment and proliferation. Since this effect is not clear in Figures SI 2-4, the cell viability 14 days after seeding NHOst on scaffolds with and without HAn was measured by image quantification (Figure SI 5). Results show that cell viability on samples with HAn are in the range of the ones without it. Besides, they support our observations pointing to a higher viability of cells seeded on PVAc containing scaffolds, exerting significant differences among PCL-HAn/PVAc group (treated and not treated with laser) vs PCL/PCL and PCL-HAn/PCL groups. Laser treated scaffolds also displayed higher viability percentages than the not treated ones highlighting the laser treatment as an improvement for cell attachment and viability.

To our knowledge, this is the first time that the incorporation of PVAc to PCL electrospun scaffolds and treated with laser to enhance their suitability in biomedical applications has been

shown these promising effects regarding human osteoblasts adhesion and proliferation, pointing to its potential application in bone repair approaches.

4. CONCLUSIONS

Rod shaped hydroxyapatite nanoparticles were successfully synthesized and incorporated into core-shell PCL/PCL and PCL/PVAc electrospun nanofibers. Only HAn loaded fibers presented hydroxyapatite precipitation after been soaked in SBF for 14 and 30 days. The presence HAn particles would be necessary for the apatite formation on the nanofiber surface. Fibers with PVAc shell suffer some structural change but they still exhibited a well interconnected pore network structure. Even when human osteoblasts growth was observed on all seeded surface, the laser treatment of the surfaces notably increased the scaffolds biocompatibility observing higher viability and cell density. This effect was more important on PCL-HAn/PVAc scaffolds with 50-90 μm micropores than on PCL-HAn/PCL (pores of 70-120 μm) suggesting that smaller micropore sizes favour cell adhesion and proliferation.

ACKNOWLEDGMENT

Authors thanks to the Ministerio de Economia y Competitividad, CTQ2014-52384-R (Spain) for the financial support. J.A. acknowledges support by EUDIME.

Funding Sources

This work was supported by the MINISTERIO DE ECONOMIA Y COMPETITIVIDAD. SPAIN (grant number CTQ2014-52384-R).

REFERENCES

Abdal-hay, A., Hamdy, A.S., Khalil, K.A., Lim, J.H., 2015. A novel simple one-step air jet spinning approach for deposition of poly(vinyl acetate)/hydroxyapatite composite nanofibers on Ti implants. Materials Science and Engineering: C 49, 681-690.

An, L., Li, W., Xu, Y., Zeng, D., Cheng, Y., Wang, G., 2016. Controlled additive-free hydrothermal synthesis and characterization of uniform hydroxyapatite nanobelts. Ceramics International 42, 3104-3112.

Aragon, J., Gonzalez, R., Fuentes, G., Palin, L., Croce, G., Viterbo, D., 2011. Development and Characterization of a Novel Bioresorbable and Bioactive Biomaterial Based on Polyvinyl Acetate, Calcium Carbonate and Coralline Hydroxyapatite. Materials Research-Ibero-American Journal of Materials 14, 25-30.

Baker, S.R., Banerjee, S., Bonin, K., Guthold, M., 2016. Determining the mechanical properties of electrospun poly-ε-caprolactone (PCL) nanofibers using AFM and a novel fiber anchoring technique. Materials Science and Engineering: C 59, 203-212.

Cramariuc, B., Cramariuc, R., Scarlet, R., Manea, L.R., Lupu, I.G., Cramariuc, O., 2013. Fiber diameter in electrospinning process. Journal of Electrostatics 71, 189-198.

Chang, K.-Y., Hung, L.-H., Chu, I.M., Ko, C.-S., Lee, Y.-D., 2010. The application of type II collagen and chondroitin sulfate grafted PCL porous scaffold in cartilage tissue engineering. J. Biomed. Mater. Res. Part A 92A, 712-723.

Chen, H., Gigli, M., Gualandi, C., Truckenmüller, R., van Blitterswijk, C., Lotti, N., Munari, A., Focarete, M.L., Moroni, L., 2016. Tailoring chemical and physical properties of fibrous scaffolds from block copolyesters containing ether and thio-ether linkages for skeletal differentiation of human mesenchymal stromal cells. Biomaterials 76, 261-272.

Choi, H.W., Johnson, J.K., Nam, J., Farson, D.F., Lannutti, J., 2007. Structuring electrospun polycaprolactone nanofiber tissue scaffolds by femtosecond laser ablation. Journal of Laser Applications 19, 225-231.

Chu, S.F., Huang, M.T., Ou, K.L., Sugiatno, E., Cheng, H.Y., Huang, Y.H., Chiu, W.T., Liou, T.H., 2016. Enhanced biocompatible and hemocompatible nano/micro porous surface as a biological scaffold for functionalizational and biointegrated implants. Journal of Alloys and Compounds 684, 726-732.

Dai, C.-F., Li, S.-P., Li, X.-D., 2015. Synthesis of nanostructured methotrexate/hydroxyapatite: Morphology control, growth mechanism, and bioassay explore. Colloids and Surfaces B: Biointerfaces 136, 262-271.

Dash, T.K., Konkimalla, V.B., 2012. Poly-ϵ-caprolactone based formulations for drug delivery and tissue engineering: A review. Journal of Controlled Release 158, 15-33.

David Nunez, J., Benito, A.M., Gonzalez, R., Aragon, J., Arenal, R., Maser, W.K., 2014. Integration and bioactivity of hydroxyapatite grown on carbon nanotubes and graphene oxide. Carbon 79, 590-604.

Ha, Y.-M., Amna, T., Kim, M.-H., Kim, H.-C., Hassan, M.S., Khil, M.-S., 2013. Novel silicificated PVAc/POSS composite nanofibrous mat via facile electrospinning technique: Potential scaffold for hard tissue engineering. Colloids and Surfaces B: Biointerfaces 102, 795-802.

Jing, X., Jin, E., Mi, H.-Y., Li, W.-J., Peng, X.-F., Turng, L.-S., 2015. Hierarchically decorated electrospun poly(epsilon-caprolactone)/nanohydroxyapatite composite nanofibers for bone tissue engineering. Journal of Materials Science 50, 4174-4186.

Joshi, M.K., Pant, H.R., Tiwari, A.P., Maharjan, B., Liao, N., kim, H.J., Park, C.H., Kim, C.S., 2016. Three-dimensional cellulose sponge: Fabrication, characterization, biomimetic mineralization, and in vitro cell infiltration. Carbohydrate Polymers 136, 154-162.
Kim, M.S., Kim, G., 2014a. Electrohydrodynamic Jet Process for Pore-Structure-Controlled 3D Fibrous Architecture As a Tissue Regenerative Material: Fabrication and Cellular Activities. Langmuir 30, 8551-8557.
Kim, M.S., Kim, G.H., 2014b. Highly porous electrospun 3D polycaprolactone/β-TCP biocomposites for tissue regeneration. Materials Letters 120, 246-250.
Kim, M.S., Son, J., Lee, H., Hwang, H., Choi, C.H., Kim, G., 2014. Highly porous 3D nanofibrous scaffolds processed with an electrospinning/laser process. Current Applied Physics 14, 1-7.
Kim, T.G., Chung, H.J., Park, T.G., 2008. Macroporous and nanofibrous hyaluronic acid/collagen hybrid scaffold fabricated by concurrent electrospinning and deposition/leaching of salt particles. Acta Biomaterialia 4, 1611-1619.
Kokubo, T., Takadama, H., 2006. How useful is SBF in predicting in vivo bone bioactivity? Biomaterials 27, 2907-2915.
Lee, B.L.-P., Jeon, H., Wang, A., Yan, Z., Yu, J., Grigoropoulos, C., Li, S., 2012. Femtosecond laser ablation enhances cell infiltration into three-dimensional electrospun scaffolds. Acta Biomaterialia 8, 2648-2658.
Liu, X., Zhao, K., Gong, T., Song, J., Bao, C., Luo, E., Weng, J., Zhou, S., 2014. Delivery of Growth Factors Using a Smart Porous Nanocomposite Scaffold to Repair a Mandibular Bone Defect. Biomacromolecules 15, 1019-1030.
Mary, I.R., Sonia, S., Viji, S., Mangalaraj, D., Viswanathan, C., Ponpandian, N., 2016. Novel multiform morphologies of hydroxyapatite: Synthesis and growth mechanism. Applied Surface Science 361, 25-32.
McCullen, S.D., Gittard, S.D., Miller, P.R., Pourdeyhimi, B., Narayan, R.J., Loboa, E.G., 2011. Laser Ablation Imparts Controlled Micro-Scale Pores in Electrospun Scaffolds for Tissue Engineering Applications. Annals of Biomedical Engineering 39, 3021-3030.
Metwally, H.A., Ardazishvili, R.V., Severyukhina, A.N., Zaharevich, A.M., Skaptsov, A.A., Venig, S.B., Sukhorukov, G.B., Gorin, D.A., 2015. The Influence of Hydroxyapatite and Calcium Carbonate Microparticles on the Mechanical Properties of Nonwoven Composite Materials Based on Polycaprolactone. Bionanoscience 5, 22-30.
Mohandes, F., Salavati-Niasari, M., Fathi, M., Fereshteh, Z., 2014. Hydroxyapatite nanocrystals: Simple preparation, characterization and formation mechanism. Materials Science and Engineering: C 45, 29-36.
Morelli, S., Salerno, S., Holopainen, J., Ritala, M., De Bartolo, L., 2015. Osteogenic and osteoclastogenic differentiation of co-cultured cells in polylactic acid-nanohydroxyapatite fiber scaffolds. Journal of Biotechnology 204, 53-62.
Nathanael, A.J., Seo, Y.H., Oh, T.H., 2015. PVP Assisted Synthesis of Hydroxyapatite Nanorods with Tunable Aspect Ratio and Bioactivity. Journal of Nanomaterials.
Ortiz, R., Moreno-Flores, S., Quintana, I., Vivanco, M., Sarasua, J.R., Toca-Herrera, J.L., 2014. Ultra-fast laser microprocessing of medical polymers for cell engineering applications. Materials Science and Engineering: C 37, 241-250.
Paz, A., Guadarrama, D., Lopez, M., Gonzalez, J.E., Brizuela, N., Aragon, J., 2012. A COMPARATIVE STUDY OF HYDROXYAPATITE NANOPARTICLES SYNTHESIZED BY DIFFERENT ROUTES. Quimica Nova 35, 1724-1727.

Pereira, I.H.L., Ayres, E., Averous, L., Schlatter, G., Hebraud, A., Chagas de Paula, A.C., Leroy Viana, P.H., Goes, A.M., Orefice, R.L., 2014. Differentiation of human adipose-derived stem cells seeded on mineralized electrospun co-axial poly(epsilon-caprolactone) (PCL)/gelatin nanofibers. Journal of Materials Science-Materials in Medicine 25, 1137-1148.
Rajzer, I., Menaszek, E., Kwiatkowski, R., Chrzanowski, W., 2014. Bioactive nanocomposite PLDL/nano-hydroxyapatite electrospun membranes for bone tissue engineering. Journal of Materials Science-Materials in Medicine 25, 1239-1247.
Rebollar, E., Cordero, D., Martins, A., Chiussi, S., Reis, R.L., Neves, N.M., León, B., 2011. Improvement of electrospun polymer fiber meshes pore size by femtosecond laser irradiation. Applied Surface Science 257, 4091-4095.
Roosa, S.M.M., Kemppainen, J.M., Moffitt, E.N., Krebsbach, P.H., Hollister, S.J., 2010. The pore size of polycaprolactone scaffolds has limited influence on bone regeneration in an in vivo model. J. Biomed. Mater. Res. Part A 92A, 359-368.
Rosales-Leal, J.I., Rodriguez-Valverde, M.A., Mazzaglia, G., Ramon-Torregrosa, P.J., Diaz-Rodriguez, L., Garcia-Martinez, O., Vallecillo-Capilla, M., Ruiz, C., Cabrerizo-Vilchez, M.A., 2010. Effect of roughness, wettability and morphology of engineered titanium surfaces on osteoblast-like cell adhesion. Colloids and Surfaces a-Physicochemical and Engineering Aspects 365, 222-229.
Sadato, A., Taki, W., Ikada, Y., Nakahara, I., Yamashita, K., Matsumoto, K., Tanaka, M., Kikuchi, H., Doi, Y., Noguchi, T., Inada, T., 1994. Experimental study and clinical use of poly(vinyl acetate) emulsion as liquid embolisation material. Neuroradiology 36, 634-641.
Singh, R.K., Jin, G.-Z., Mahapatra, C., Patel, K.D., Chrzanowski, W., Kim, H.-W., 2015. Mesoporous Silica-Layered Biopolymer Hybrid Nanofibrous Scaffold: A Novel Nanobiomatrix Platform for Therapeutics Delivery and Bone Regeneration. ACS Applied Materials & Interfaces 7, 8088-8098.
Song, W., Yu, X., Markel, D.C., Shi, T., Ren, W., 2013. Coaxial PCL/PVA electrospun nanofibers: osseointegration enhancer and controlled drug release device. Biofabrication 5.
Suwantong, O., Pankongadisak, P., Deachathai, S., Supaphol, P., 2014. Electrospun poly(L-lactic acid) fiber mats containing crude Garcinia mangostana extracts for use as wound dressings. Polymer Bulletin 71, 925-949.
Taheri, M.M., Abdul Kadir, M.R., Shokuhfar, T., Hamlekhan, A., Assadian, M., Shirdar, M.R., Mirjalili, A., 2015. Surfactant-assisted hydrothermal synthesis of Fluoridated Hydroxyapatite nanorods. Ceramics International 41, 9867-9872.
Uma Maheshwari, S., Samuel, V.K., Nagiah, N., 2014. Fabrication and evaluation of (PVA/HAp/PCL) bilayer composites as potential scaffolds for bone tissue regeneration application. Ceramics International 40, 8469-8477.
Verma, G., Barick, K.C., Manoj, N., Sahu, A.K., Hassan, P.A., 2013. Rod-like micelle templated synthesis of porous hydroxyapatite. Ceramics International 39, 8995-9002.
Wang, J., Valmikinathan, C.M., Liu, W., Laurencin, C.T., Yu, X., 2010. Spiral-structured, nanofibrous, 3D scaffolds for bone tissue engineering. J. Biomed. Mater. Res. Part A 93A, 753-762.
Wu, Y., Vorobyev, A.Y., Clark, R.L., Guo, C., 2011. Femtosecond laser machining of electrospun membranes. Applied Surface Science 257, 2432-2435.
Zhang, Y., Gu, J., Tan, H., Shi, J., Di, M., Zuo, Y., Qiu, S., 2013. Preparation and characterization of film of poly vinyl acetate ethylene copolymer emulsion. Applied Surface Science 276, 223-228.

Figure Captions

Figure 1: Characterization of the synthesized HAn: a) XRD, b) SEM images, c) TEM micrographs, d) FTIR spectrum.

Figure 2: XRD patterns of PCL/PCL, PCL/PVAc, PCL-HAn/PCL and PCL-HAn/PVAc fibers

Figure 3: SEM images of a) PCL/PCL fiber, b) PCL-HAn/PCL fibers.

Figure 4: TEM images of a) PCL/PVAc fiber, inset PCL/PCL fiber, b) PCL-HAn/PVAc fiber.

Figure 5: SEM images and pore size distribution of laser treated a) and c) PCL-HAn/PCL and b) and d PCL-HAn/PVAc) .

Figure 6: SEM images of the prepared materials after immersion in SBF solution during different times.

Figure 7: SEM micrographs showing the morphology and adhesion of human osteoblasts seeded onto the different prepared materials at different time points (2, 7 and 14 days after cell seeding). Scale bars 100nm.

Figure 8: Confocal microscope images of scaffolds surface (left) and viability (right) of human osteoblasts seeded in PCL-HAn/PVAc scaffolds not treated (above) and treated with laser (below) after 14 days of cell seeding. Scale bars 100µm.

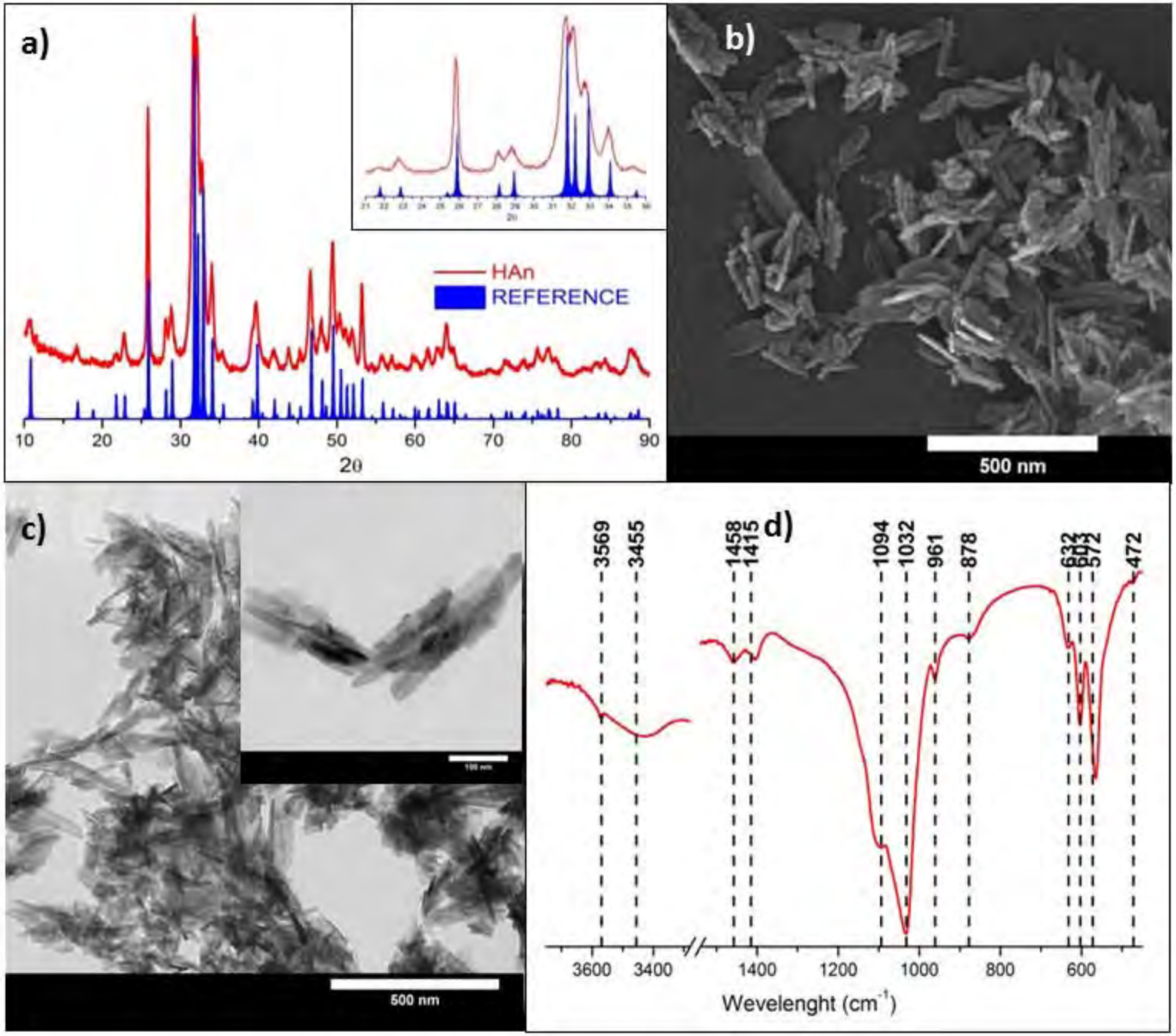
a)
HAn
REFERENCE
10
20
30
40
50
60
70
80
90
2θ
b)
500 nm
c)
500 nm
d)
3569
3455
1458
1415
1094
1032
961
878
632
603
572
472
3600
3400
1400
1200
1000
800
600
Wevelenght (cm-1)

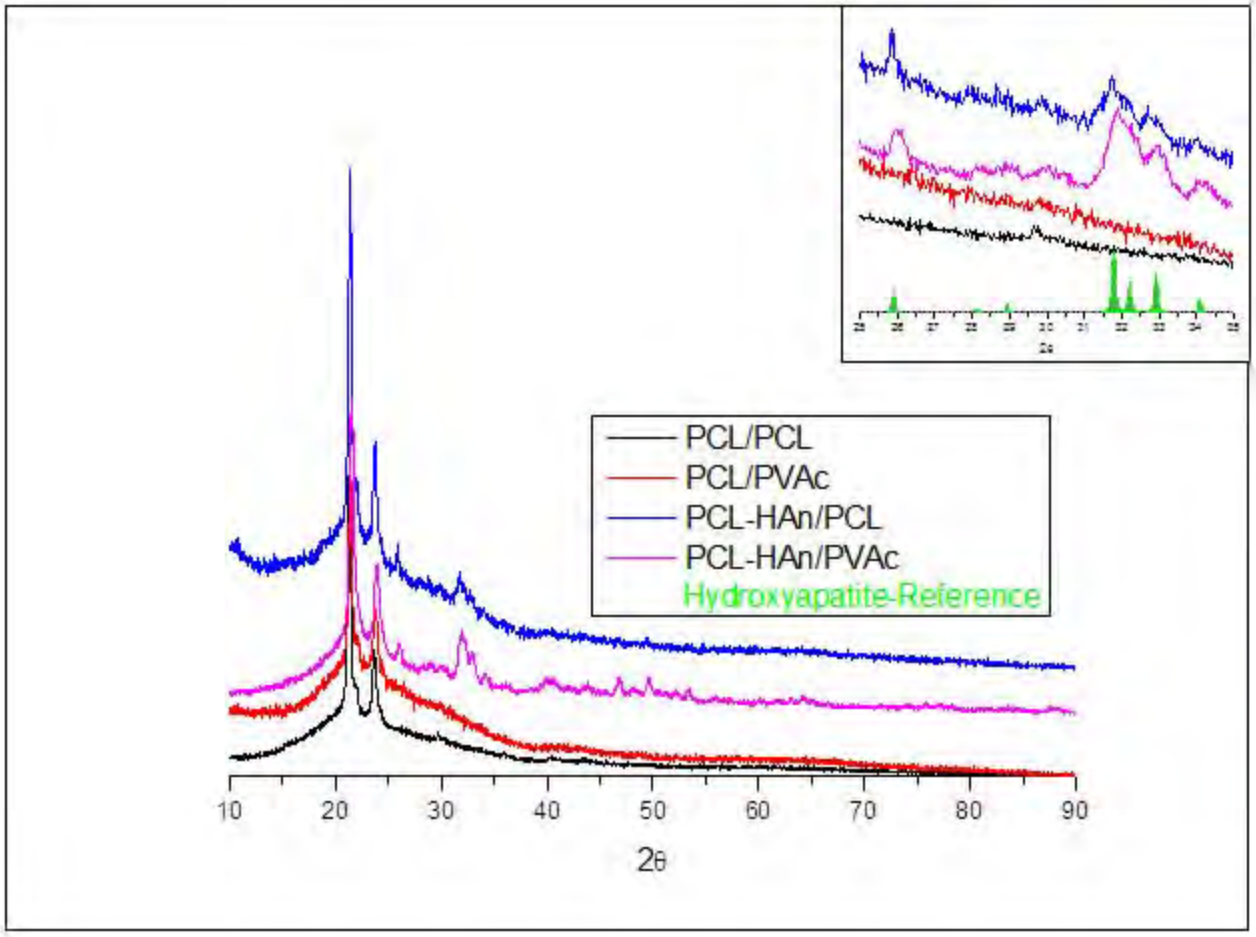
PCL/PCL
PCL/PVAc
PCL-HAn/PCL
PCL-HAn/PVAc
Hydroxyapatite-Reference
10
20
30
40
50
60
70
80
90
2θ

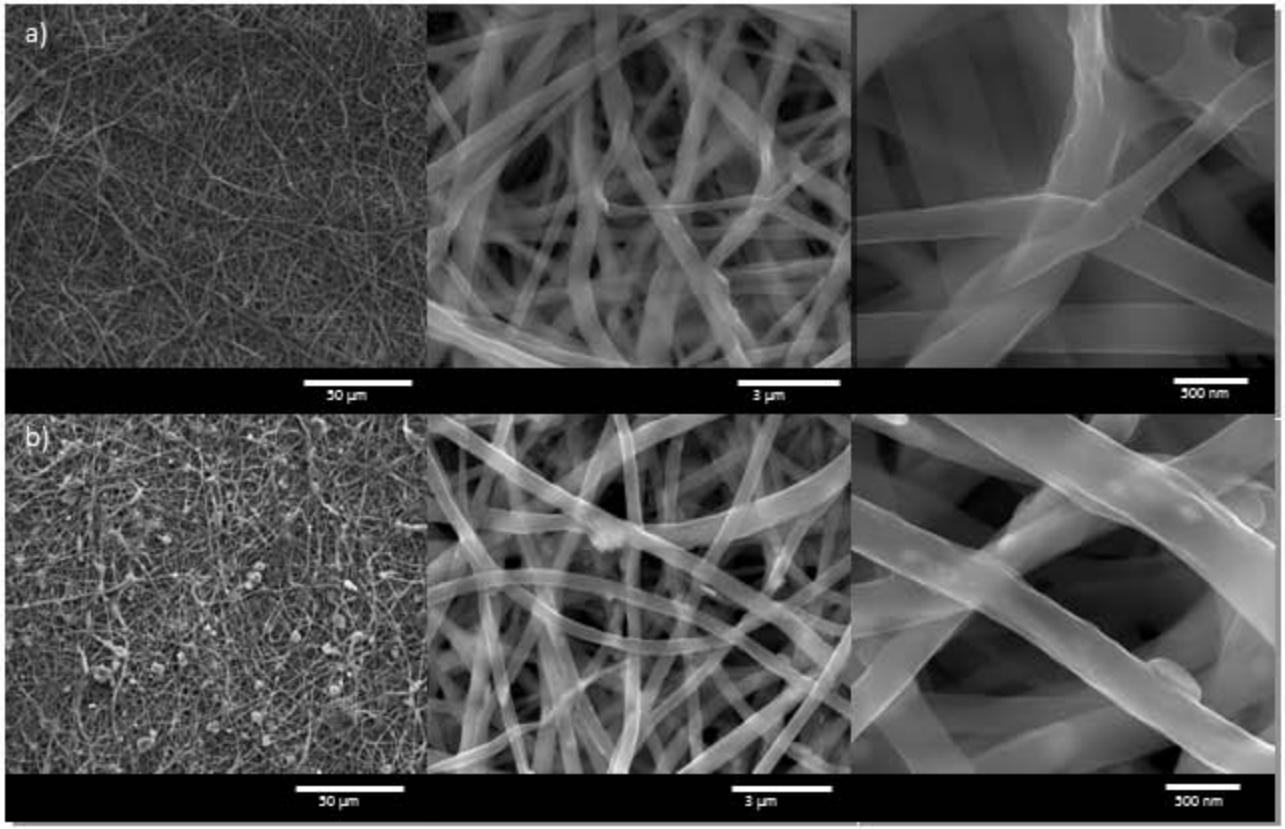
a)
50 µm
3 µm
500 nm
b)
50 µm
3 µm
500 nm

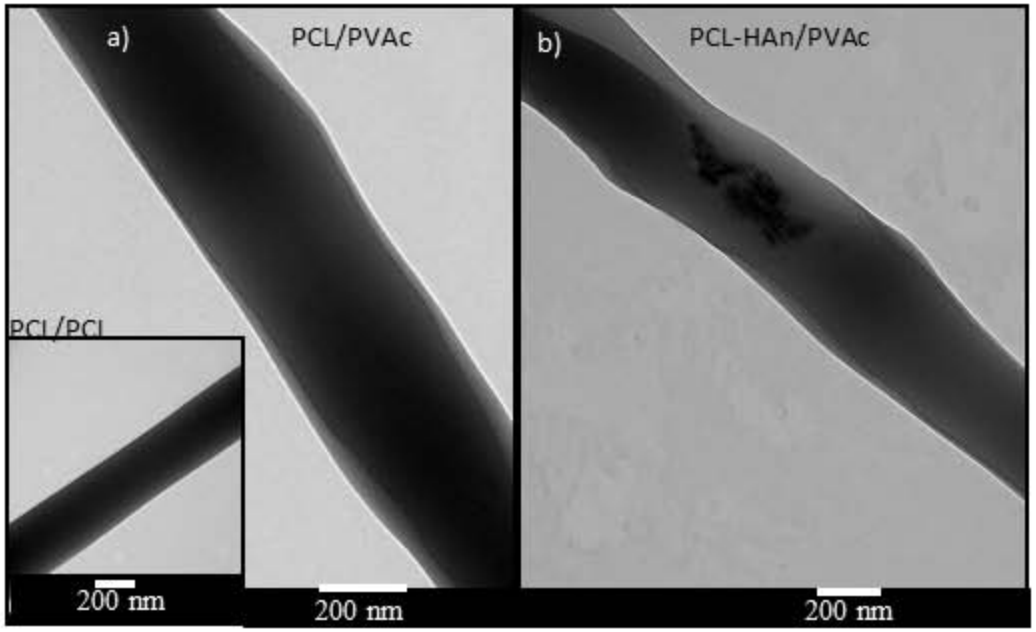
a)
PCL/PVAc
PCL/PCL
200 nm
200 nm
b)
PCL-HAn/PVAc
200 nm

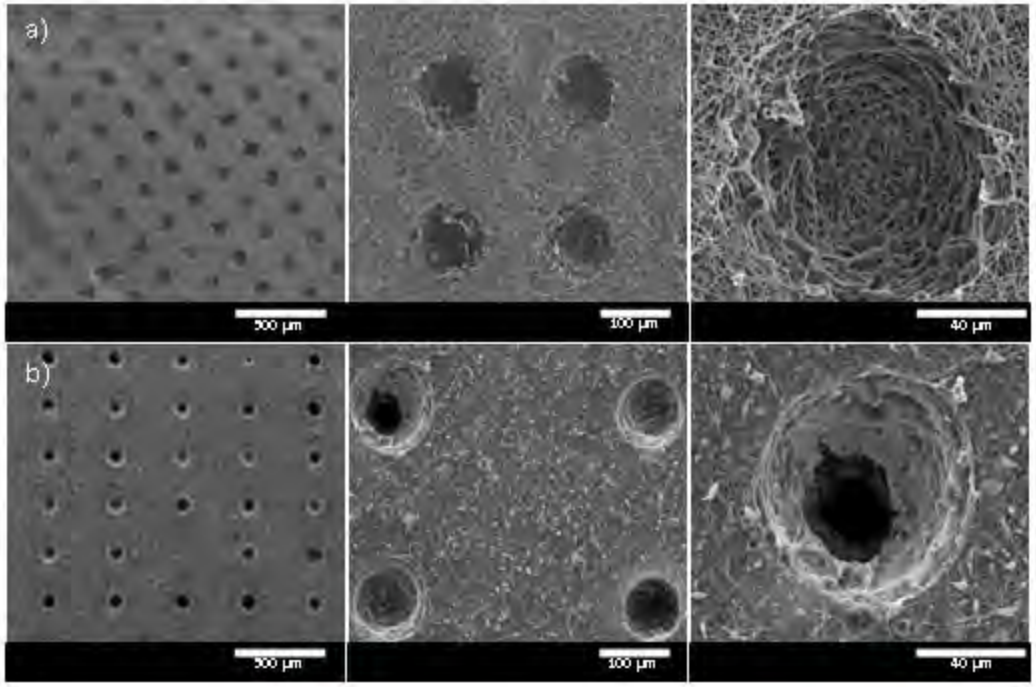
a)
500 µm
100 µm
40 µm
b)
500 µm
100 µm
40 µm

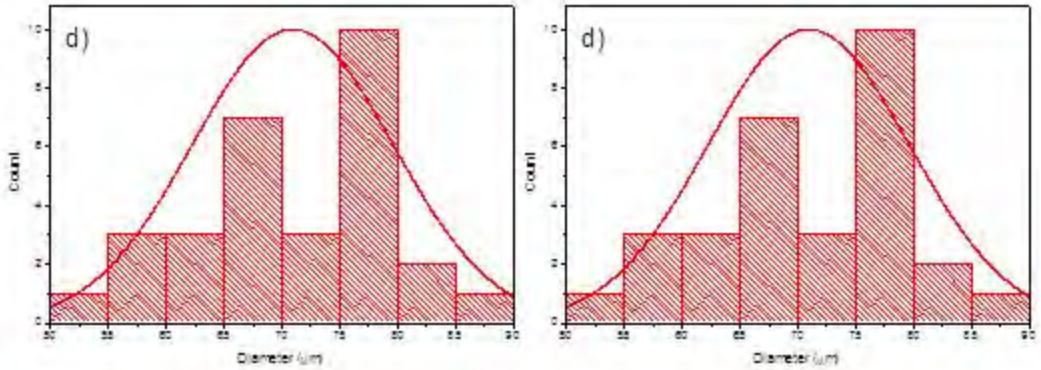
d)
Count
Diameter (µm)
d)
Count
Diameter (µm)

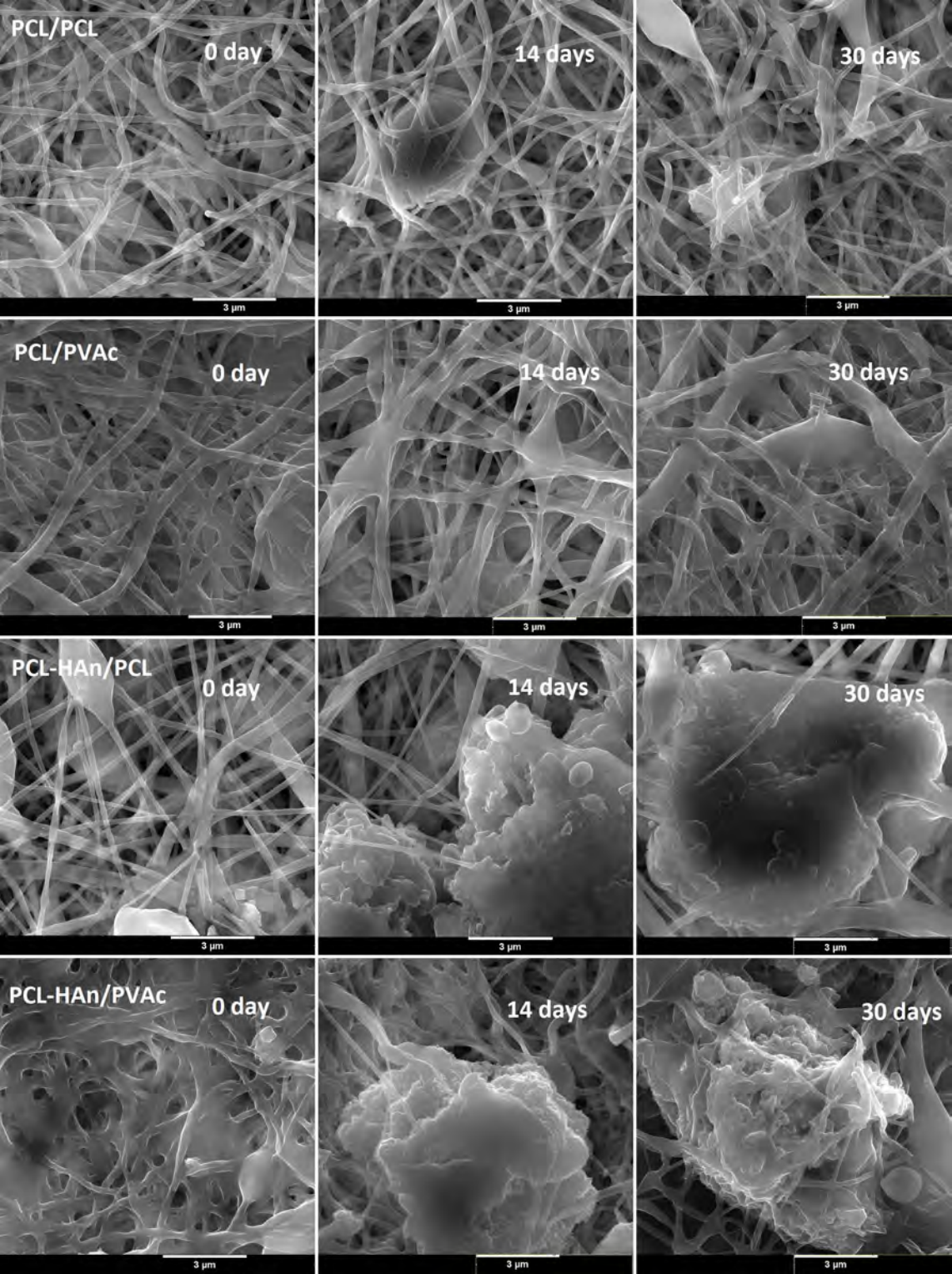
PCL/PCL
0 day
14 days
30 days
PCL/PVAc
0 day
14 days
30 days
PCL-HAn/PCL
0 day
14 days
30 days
PCL-HAn/PVAc
0 day
14 days
30 days
3 µm

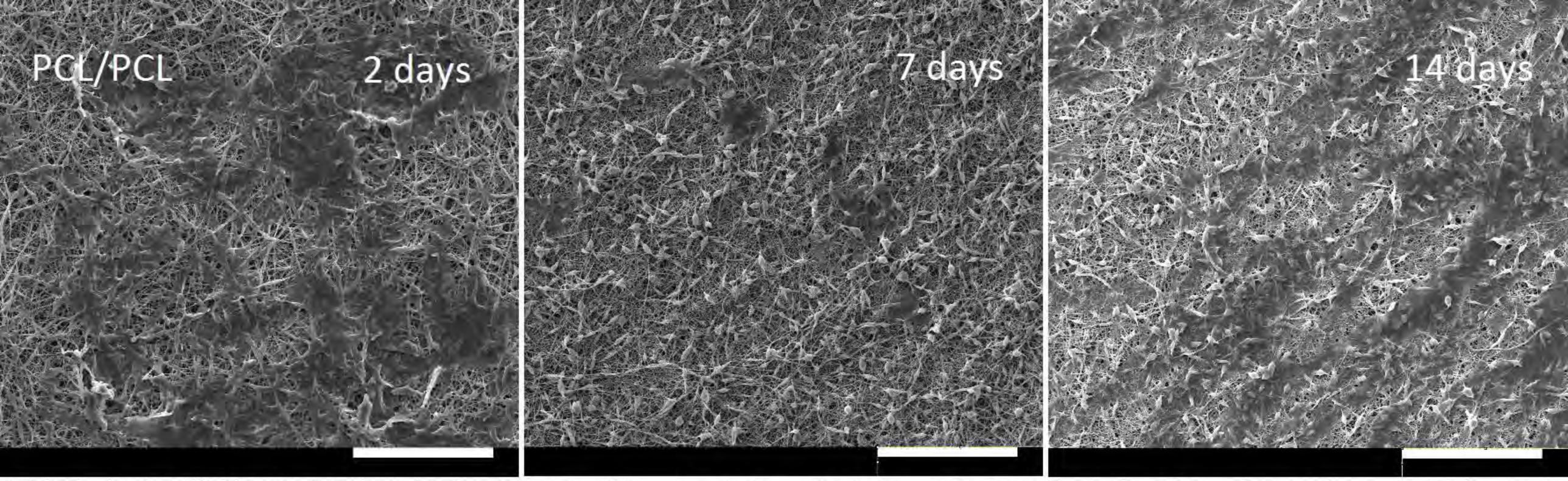
PCL/PCL
2 days
7 days
14 days
PCL/PVAc
2 days
7 days
14 days
PCL-HAn/PCL
2 days
7 days
14 days
PCL-HAn/PVAc
2 days
7 days
14 days

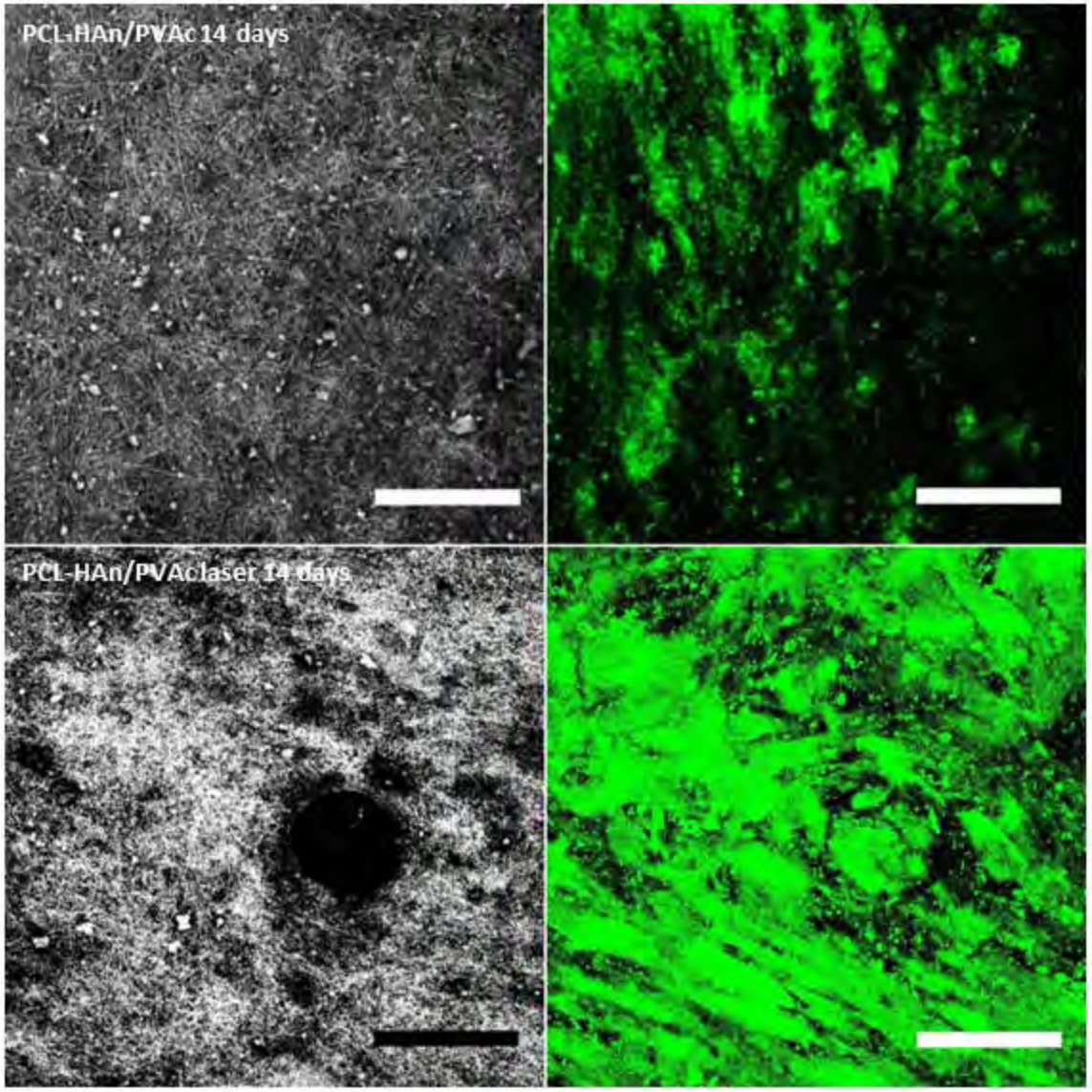
PCL-HAn/PVAc 14 days
PCL-HAn/PVAclaser 14 days